Phys. Status Solidi A **208**, No. 6, 1357–1363 (2011) / **DOI** 10.1002/pssa.201001199

physica status solidi a
www.pss-a.com
applications and materials science

# Miniaturised eight-channel impedance spectroscopy unit as sensor platform for biosensor applications

**Jeroen Broeders[*,1,2], Stijn Duchateau[2], Bart Van Grinsven[1], Wouter Vanaken[2], Marloes Peeters[1], Thomas Cleij[2], Ronald Thoelen[2], Patrick Wagner[1,3], and Ward De Ceuninck[**,1,3]**

[1] Institute for Materials Research, Hasselt University, Wetenschapspark 1, 3590 Diepenbeek, Belgium
[2] Xios University College, Agoralaan Gebouw H, 3590 Diepenbeek, Belgium
[3] IMEC, Devision IMOMEC, Wetenschapspark 1, 3590 Diepenbeek, Belgium

Received 29 October 2010, revised 27 January 2011, accepted 2 February 2011
Published online 9 May 2011

**Keywords** biosensors, electrochemical analysis, impedance spectroscopy, molecular imprinting

[*] Corresponding author: e-mail jeroen.broeders@uhasselt.be, Phone: +32-011-26-88-35, Fax: +32-011-26-88-99
[**] e-mail ward.deceuninck@uhasselt.be

A miniaturised, low cost impedance analyser is developed to ease the use of impedance spectroscopy in biological setups. This could form the first step towards fully standalone, hand-held biosensor applications. The system is capable of performing quasi-simultaneous time resolved impedance measurements on eight different channels in a frequency range of 10 Hz–100 kHz. The unit is accurate in a broad impedance range and is able to perform stable measurements over intervals of several days. The system is characterised by passive components, a temperature controlled wet cell based impedance setup and a biomimetic molecularly imprinted polymer (MIP) based histamine sensor. The test results all indicate accurate and stable functioning of the unit, making it suitable for bioanalytical applications.



**1 Introduction** Impedance spectroscopy can be used as a readout technique for a wide variety of sensors. The technique has already been used with success for monitoring DNA hybridisation and detection of single nucleotide polymorphisms [1], nicotine and histamine recognition by means of molecularly imprinted polymers (MIPs) [2–4] and the detection of immunoreactions [5–7]. Furthermore, impedance spectroscopy is used as a reference for other biosensor readout techniques [8–10]. This measurement is usually performed by bulky, expensive equipment. To ease the readout of biosensors, a first step towards a miniaturised and low cost impedance spectroscopy unit was already developed based on the Analogue Devices AD5933 chip [11]. The main advantage of this chip was that complex measurement circuitry that is present in conventional equipment is now integrated in a single chip, resulting in a much smaller unit. The integration of the measurement circuitry in a chip also decreases noise caused by signal paths between separate electronic components. This device was capable of performing impedance measurements in a range of 10 Ω–2 MΩ in a frequency spectrum of 100 Hz–100 kHz [12]. Although the unit is capable of performing stable measurements on biosensors, it had some limitations in usable ranges, accuracy and ease-of-use. These problems have now been overcome in the new system.

The setup is downscaled to a hand-held device and is being interfaced by USB to a computer, which also provides power for the system. This eliminates the need for any external power supply. The frequency bandwidth has been increased from 10 Hz to 100 kHz, with sub-Hertz resolution. The measurable impedance ranges from 10 Ω to 5 MΩ. Figure 1 shows this newly developed device, with a 1 Euro coin placed on top for size reference. One can clearly distinguish the 16 subminiature coax SMB connectors on top, which are used for connection to samples, and the USB- and peripheral port on the side of the device.

The applicability of the developed system, both in electronic lab setup as well as under biological research conditions was investigated.

## 2 Experimental

**2.1 Measurement setup** As can be seen in Fig. 2, the unit has an on-board $I^2C$-bus which controls all measurement- and peripheral circuitry. This bus is interfaced

**Figure 1** (online colour at: www.pss-a.com) The developed eight-channel impedance analyser with USB-port and SMB connectors visible.

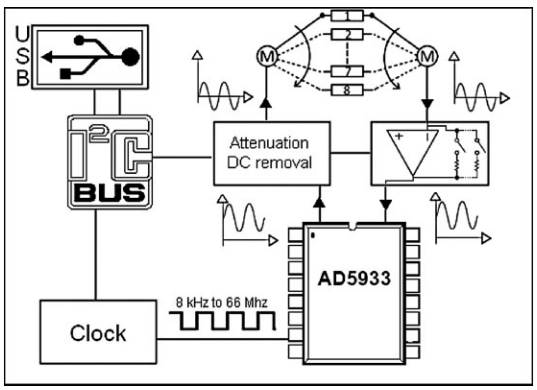


**Figure 2** Simplified diagram of the measurement circuit.

to an USB-port by a Future Technologies Devices International (FTDI) chip, enabling full control over the circuitry via USB protocol [13]. The measurement circuitry alters the signal generated by the impedance chip, which is a sine wave with a minimal peak-to-peak voltage of 198 mV and a bias of 173 mV, to a usable signal for biological measurements. This includes removal of the bias voltage by means of a single capacitor and attenuation of the signal in a voltage divider to avoid polarisation of the electrodes. The result is a 65 mV peak-to-peak sine wave oscillating voltage and a 0 V bias voltage. It is however possible to further decrease the voltage by fine-tuning an on-board potentiometer connected to the voltage divider. This can be, for example necessary when performing measurements on biological cells which have an action potential of 60 mV and will trigger ion channels when bigger voltages are applied [14].

The resulting current, caused by the impedance of the sample, is converted to a voltage by an inverting operational amplifier (opamp) circuit. With a fixed feedback resistor connected to this opamp, the AD5933 chip is by itself only capable of analysing samples within a fixed impedance range. Since the impedance of the sample can vary strongly during biological measurements [15, 16], the amplification factor of the opamp will also vary strongly, which may cause the output voltage of the opamp to go either out of range of the impedance chip or become too small to analyse. This was overcome by a set of resistors which can be connected as feedback resistor using mechanical relay switches. Software controls the selection of the suited feedback resistor during measurements, keeping the amplification factor and output voltage of the opamp in a suitable range for analysis by the AD5933 chip. A calibration sequence, which is performed before every measurement, delivers a set of correction factors which are utilised to compensate for the different feedback resistors. As a last step in the signal chain the bias voltage is again added by means of a time- and temperature-stable Zener diode.

Peripheral circuitry inside the unit includes precise clocking to enable measurements in a wide frequency spectrum. The optimal frequency at which impedance spectroscopy is performed in biological applications is strongly dependant on the specific purpose. Examples include a frequency of 80 Hz for polymer-based immunosensors [6], a kilohertz range for DNA and cell-based sensors [17, 18] and 1 MHz for diamond based C-reactive protein (CRP) sensors [5]. The internal clocking oscillator inside the chip, which determines the sampling frequency in the analogue-to-digital convertor (ADC) and thus the analysable frequency range, has a fixed frequency of 16.66 MHz. Since 1024 samples are needed for discrete Fourier transformation (DFT) inside the chip, the minimal detectable frequency lies at 16 kHz. A Maxim Integrated Products clock chip with a programmable frequency ranging from 10 kHz to 66 MHz was used as external clocking device for the impedance analyser [19]. This results in a lowest analysable frequency of 10 Hz. It should also be noted that the AD5933 chip is, on itself, only capable of performing linear frequency sweeps. Since the frequency range has been extended to four decades, a logarithmic sweep would be preferred. This has been achieved by softwarematically forcing the chip to perform a series of single-frequency measurements which are logarithmically divided along the complete frequency range.

The power of the unit is supplied by the USB-port of 5 V, which is stabilised by voltage regulators. On board analogue and digital voltage are separated to avoid influence of the digital components, for example noise generated by the clocking chip, on the analogue measurement circuitry. The eight different input channels are double pole switched by mechanical relays, controlled by software, to avoid interference between samples via the analyser.

Interfacing to the sensor platforms is performed by subminiature SMB connectors, with shielding connected to the ground of the circuit, or zero-insertion-force (ZIF) sockets. A peripheral port, which supplies voltages and $I^2C$ protocol, enables usage of the device in a master-slave setup with other equipment, e.g. external multiplexers.

**2.2 General characterisation** First, a general characterisation is performed, by measuring electrical

 

resistors with a resistance ranging from 10 Ω to 820 kΩ and a series resistor–capacitor circuit with a metal film resistor of 33 Ω and a ceramic capacitor of 100 nF.

As a first step to analyse the accuracy of the unit a set of metal film resistors ranging from 10 Ω to 820 kΩ was measured over the complete frequency bandwidth of 10 Hz–100 kHz. This frequency range was swept logarithmically. For a measurement with ten points per decade, a frequency sweep of 40 frequency points was performed within 20 s. The measurement time on biological samples can vary from a few minutes, in for example DNA sensors [20], to several days in cell growth studies [21]. Therefore, the long-term stability of the unit is also an important factor. A series resistor–capacitor circuit with a metal film resistor of 33 Ω and a ceramic capacitor of 100 nF was measured over 60 h. The standard deviation of the measured impedances was calculated per frequency point over time.

**2.3 Wet cell condition** Biological measurements are often performed under wet cell conditions at different temperatures. These temperatures include room temperature, 37 °C for *in vivo* applications and 70–80 °C for real-time monitoring of DNA hybridisation [1, 22]. Therefore, the unit should not only function properly when measuring solid state components, but also when measuring wet cell biosensors setups at different temperatures. To test the applicability of the unit under these conditions a prototype sensor-cell was constructed, as shown in Fig. 3. This cell utilises a silicon electrode with nanocrystalline diamond (NCD) coating and a copper back contact [23]. Diamond is biocompatible and is suited for attachment of biological receptors, enabling application as an immobilisation platform for use in biological measurements [24]. Furthermore, diamond has a high thermal conductivity, it is chemically inert and it can be made semiconducting by chemical doping [25]. A chemically inert platinum wire was used as a counter electrode. The fluid cell was sealed by a rubber O-ring with inner diameter of 7 mm, pressed onto a teflon lid with an opening of equal size. The cell was filled with 140 µl of phosphate buffered saline (PBS) solution, a commonly used salt solution which mimics the bloods pH and ionic strength. Furthermore, a thermocouple was mounted into the copper and a second one was mounted in the fluid, to monitor temperature. A temperature profile ranging form room temperature to 85 °C was utilised to verify the functionality of the setup in the range of biologically relevant temperatures. These temperatures were applied in steps of 10 °C at a heating rate of 0.66 °C/min by a programmable hot plate. After each step the setup was allowed to stabilise for 15 min. After reaching the maximum temperature of 85 °C the setup was again allowed to stabilise for 15 min after which the setup was cooled down by means of convection, though following the protocol as described above. This way a temperature range from 35 to 85 °C was obtained. During this process, the impedance was monitored. The working and counter electrode of the cell were connected to the impedance unit with 50 Ω coaxial cables with SMB-connectors. The impedance was monitored by performing frequency sweeps from 100 Hz to 100 kHz with ten divisions per decade, at a speed of 5 s per frequency sweep.

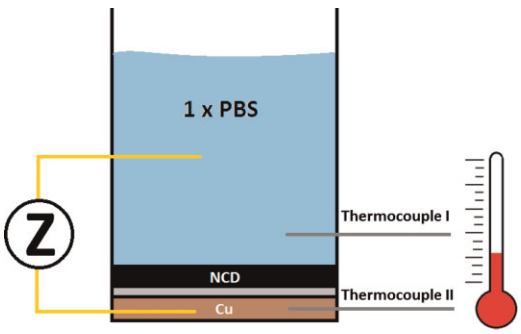


**Figure 3** (online colour at: www.pss-a.com) Experimental setup for impedimetric measurements on 1 × PBS at different temperatures (schematic).

**2.4 Biomimetic sensor** As a last step in validation of the unit in biosensor setups, a biomimetic sensor was analysed. A MIP was used to detect the concentration of histamine in a PBS solution. Histamine, a low molecular weight molecule with chemical formula $C_5H_9N_3$, plays an important role in asthma [26], allergies [27] and irritable bowel syndrome [28]. MIPs are synthetic receptors which consist of polymers in which nanocavities are present with the exact shape, size and functionality complementary to a target molecule [29, 30]. When the target molecule binds in a nanocavity, the dielectric properties of the MIP change, which can be detected by impedance spectroscopy.

Molecularly imprinted polymers suited for detection of histamine and non-imprinted polymers (NIPs), were synthesised from a mixture of methacrylic acid (17.8 mmol), ethylene glycol dimethacrylate (36 mmol) and azobisisobutyronitrile (0.60 mmol), together with the template molecule histamine (8.99 mmol), following the method described in Ref. [3]. The NIPs can be used as a reference during measurements and allow for compensation of non-specific absorption of target molecules. Since the developed device has eight measurement channels, a differential measurement can be performed on both the MIP and the NIP sample. In order to do so, a cell similar to Fig. 3 was constructed, though with two aluminium electrodes with copper back contacts. Both the MIP and the NIP sample were immobilised on these aluminium substrates. The cell was kept at a constant temperature of 37 °C with a programmable hot plate to mimic *in vivo* conditions. The sensor was allowed to stabilise for 2.5 h in the fluid cell filled with PBS, after which a concentration of 2 nM of histamine was added. Hereafter the setup was allowed to stabilise for 30 min. Impedance spectroscopy was simultaneously performed on the MIP and the NIP channel in a frequency range of 100 Hz–100 kHz at a speed of 5 s per sweep.

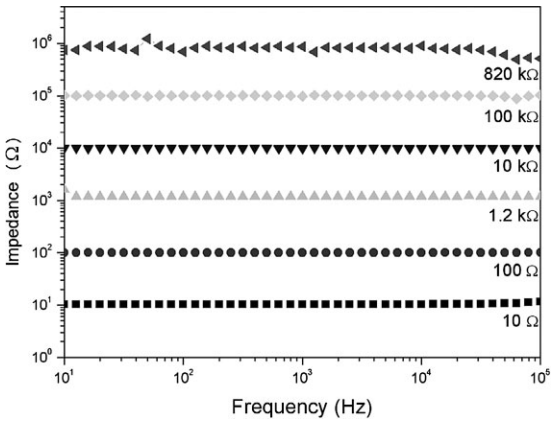


**Figure 4** Bode plots, displaying the log impedance from 10 Hz to 100 kHz, for resistors ranging from 10 Ω to 820 kΩ.

## 3 Results and discussion

**3.1 General characterisation** Measurements were performed using 40 resistors with values divided logarithmically along the range from 10 Ω to 820 kΩ. According to the specifications of the AD5933 chip used in the unit, the error is less then 0.5% for the usable impedance range. Figure 4 shows the Bode plots for a selection of the measured set of resistors, displaying the impedance as function of the frequency from 10 Hz to 100 kHz. It can be seen that it is possible to perform measurements in an impedance range from 10 Ω to 820 kΩ. It should be noted that the absolute error increases with increasing resistor value, possibly due to decreasing current and decreasing signal to noise ratio. Since the excitation voltage is limited to 65 mV, the resulting current through a 1 MΩ resistor is only 65 nA, making the measurement susceptible to noise. This noise has however no noticeable influence on samples below 100 kΩ in impedance. The long term stability of the unit was tested by measuring a series resistor–capacitor circuit for 60 h. The standard deviation was determined for each frequency by calculating the relative deviation of each measurement point in respect to the average measured impedance. Overall this standard deviation lies around 0.1%, although there are two data points that deviate significantly more than the other points. These points are situated around 50 and 100 Hz.

The 50 Hz deviation is most likely caused by interference coming from the line voltage. Although the unit is not powered by a power outlet, this interference can still enter the unit via the USB-port. Also the 100 Hz noise, which is the first harmonic of power outlet frequency, can be explained in this way. The noise introduced by the first harmonic of a signal should be significantly lower than noise caused by the frequency itself. It was observed that the deviation at 100 Hz is lower than 50 Hz deviation. This noise can however easily be solved by correct filtering of the USB-voltages entering the system.

**3.2 Wet cell condition** Impedance is measured in a frequency range of 100 Hz–100 kHz in a fluid cell while imposing a temperature profile, ranging from 35 to 85 °C. Biological effects in wet cell conditions usually occur on the interface between an immobilisation layer and an electrolyte [2, 6, 22]. This makes the interface region, and more specifically its distinct double-layer capacitance, the most interesting region for performing impedance spectroscopy. An equivalent electrical circuit of the fluid cell with values taken at room temperature is shown in Fig. 5a. The resistance of the solution present in the cell is indicated by a series resistor, while the parallel capacitor–resistor circuit is related to the interface region. The values in this circuit, together with Bode plots, indicates that the capacitance is mostly present around a frequency of 12.5 kHz. In Fig. 5b the impedance at this fixed frequency of 12.5 kHz is displayed over time as well as the measured temperatures of both copper and liquid. It can be observed clearly that the measured impedance is inversely proportional to the

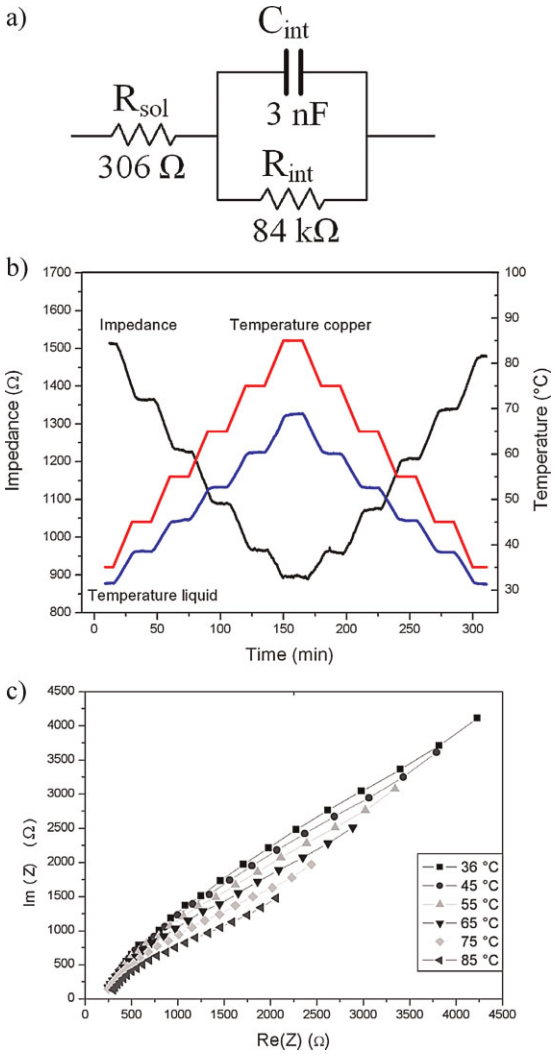


**Figure 5** (online colour at: www.pss-a.com) Equivalent electrical circuit of the liquid cell (a), impedance and temperature *versus* measurement time at a frequency of 12.5 kHz (b) and Nyquist plot of the temperature controlled measurement (c).

temperature profile, which is most likely caused by the temperature dependence of the double-layer capacitance. Figure 5c shows Nyquist plots of the impedance data from 1 to 100 kHz at temperatures of 35, 45, 55, 65, 75 and 85 °C. It becomes distinct that an increasing temperature leads not only to a decrease in the imaginary part of the Nyquist plot, but also in the real part, indicating both resistive and capacitive effects. This resistive effect is most likely caused by higher ion mobilities in the electrolyte with increasing temperature.

To gain insight into this temperature effect at different frequencies, a linear fit of the impedance at different temperatures was performed for frequencies of 1, 2, 5, 10 and 20 kHz. The data of the performed fits is shown in Table 1. The slope increases with increasing frequency indicating that the temperature effect shifts towards the imaginary part with increasing frequency. This shows a larger temperature dependence for the capacitive components, related to the interfacial double-layer, compared to the resistive solution components of the sample. This temperature effect can also be monitored in the phase, where an increase in temperature of 1 °C causes a phase shift of 0.3°.

**3.3 Biomimetic sensor** Measurements described in Section 3.2 are repeated with two aluminium working electrodes covered with a conductive polymer loaded with either MIP or NIP particles. The temperature is fixed at 37 °C in order to prevent temperature effects discussed in Section 3.2. This setup is allowed to stabilise for 100 min. Figure 6a shows the Bode plot of the stabilised MIP sample right before and 15 min after addition of histamine. An impedance difference can be clearly observed in the highest frequency decade. This effect is however also present in the NIP sample and is most likely related to a change in the electrolyte conductivity, caused by addition of the target molecule. Using the NIP sample as a reference, the intrinsic effect of histamine detection is mostly present in the first frequency decade and can be most clearly observed around 150 Hz. Equivalent circuit modelling before addition indicates a double-layer capacitance of 27 nF with a parallel charge-transfer resistance of 16 kΩ. In order to monitor the interfacial effects of target molecule binding inside the MIP cavities, both the real and imaginary part of the impedance were plotted *versus* time at a set frequency of 150 Hz. Figure 6b shows the relative variation of the real part

**Table 1** Slope and coefficient of determination for different frequencies.

| frequency (kHz) | slope | $R^2$ |
|---|---|---|
| 1 | 1.21 | 1.000 |
| 2 | 1.36 | 0.998 |
| 5 | 1.75 | 0.988 |
| 10 | 2.21 | 0.961 |
| 20 | 2.50 | 0.980 |

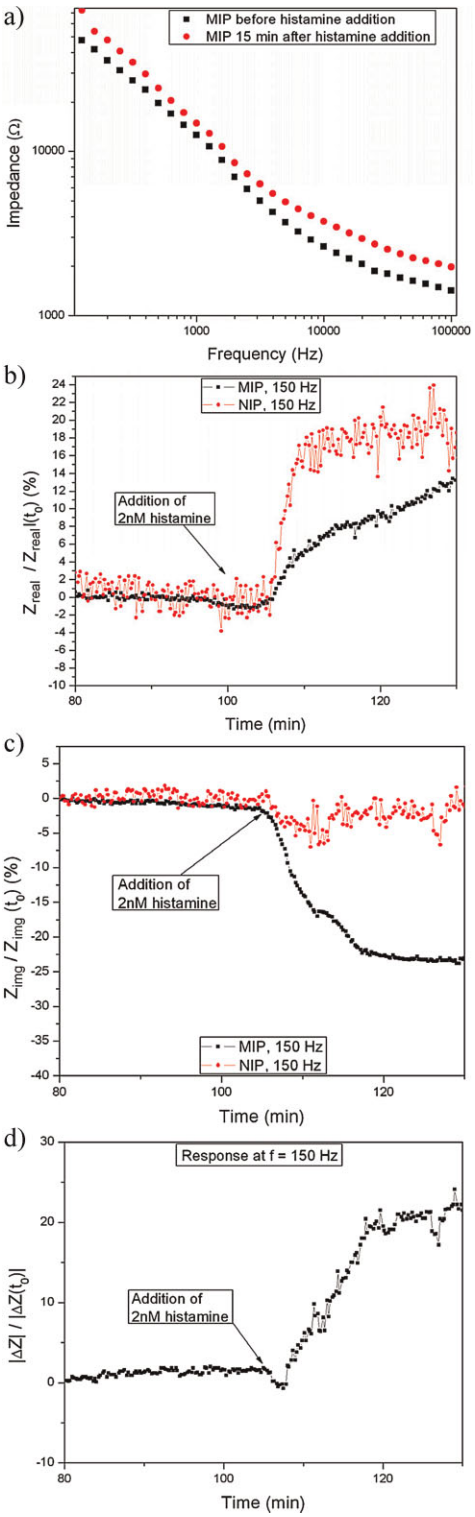


**Figure 6** (online colour at: www.pss-a.com) Bode plots of the cell with an MIP sample mounted (a), real (b) and imaginary (c) part over time and relative impedance of the MIP – NIP *versus* time (d). The impedance changes are normalised to their value 20 min before histamine was added.

of both the MIP and NIP sample, which is used as a reference, in respect to their values taken 20 min before histamine was added ($t_0$). Addition of the target molecule results in an increase in the real part of both the MIP and the NIP sample. The difference in slope is probably a result of the stabilisation period of the MIP. As can be seen in Fig. 6c, addition of the target molecule results in a decrease of the MIP imaginary part of about 15% with a decrease of 2% in the NIP sample. This is most likely caused by non-specific binding or absorption of target molecule in the NIP. This indicates that the impedance change due to binding of a target molecule in the MIP is most dominant in the imaginary part of the impedance, which is related to the interfacial double-layer capacitance. The measured impedance values were normalised relative to their initial values, resulting in a relative impedance $Z(t)/Z(t_0)$. In Fig. 6d the difference between the relative impedance signals of the MIP and the NIP is plotted over time. Addition of the 2 nM concentration of histamine causes a slight drop in impedance due to movement of the liquid, after which the impedance increases significantly in respect to the impedance of the NIP, indicating detection of the target molecule. When stabilising for 15 min after addition of the target, an increase of about 20% occurred.

**4 Conclusion** Both accuracy and stability of the developed impedance spectroscopy unit were analysed using passive components and circuits. These results show that the device is accurate in a broad impedance range and is able to perform stable measurements over intervals of several days. Measurements on a temperature controlled fluid cell indicate that the device is also capable of measuring setups for biological samples at high accuracy and stability.

As is shown in this paper, the system can clearly identify temperature differences in a cell filled with 1× PBS and a diamond electrode by monitoring the time variation of the measured impedance at certain frequencies. Nyquist plots also indicate that this temperature-driven impedance variation is present in the real as well as the imaginary part. This is most likely related to both interfacial double-layer capacitance and electrolyte conductivity. Furthermore, the system was tested with its multichannel option on a biomimetic MIP-based histamine sensor. Upon detection of a concentration as small as 2 nM of target molecule a significant change in double-layer capacitance could be monitored. These results indicate that the setup can be used for impedimetric detection of chemical binding in sensors, making it suited for bioanalytical purposes.

The unit will most likely become a vital part of current impedimetric biosensor setups. Possible applications include, amongst others, DNA single nucleotide mismatch identification, detection of antibody–antigen recognition and impedimetric cell growth measurements. There is still room for improving biosensor measurement setups and the developed unit may become the first step towards fully standalone, portable biosensor applications. Furthermore, this setup can be used in any field of research where impedance spectroscopy is used and its low cost and small size offers advantages over conventional equipment. Additional improvements could be achieved by further extending the impedance range by adding feedback resistors to the circuit, and lowering the minimal excitation frequency by altering the clocking signal. This could enable the use in an even wider range of applications.

**Acknowledgements** We would like to thank the Special Research Funds of Hasselt University and Xios University College to provide us with the necessary financial resources. Furthermore, we owe thanks to Jan Mertens, Johan Sogen, Johnny Baccus and Lieven De Winter for technical support and Hannelore Strauven for assisting during measurements.

## References

[1] V. Vermeeren, N. Bijnens, S. Wenmackers, M. Daenen, K. Haenen, O. A. Williams, M. Ameloot, M. vandeVen, P. Wagner, and L. Michiels, Langmuir **23**, 13193–13202 (2007).
[2] R. Thoelen, R. Vansweevelt, J. Duchateau, F. Horemans, J. D'Haen, L. Lutsen, D. Vanderzande, M. Ameloot, M. vandeVen, T. Cleij, and P. Wagner, Biosens. Bioelectron. **23**, 913–918 (2008).
[3] E. Bongaers, J. Alenus, F. Horemans, A. Weustenraed, L. Lutsen, D. Vanderzande, T. J. Cleij, F. J. Troost, R.-J. Brummer, and P. Wagner, Phys. Status Solidi A **207**, 837–843 (2010).
[4] F. Horemans, J. Alenus, E. Bongaers, A. Weustenraed, R. Thoelen, J. Duchateau, L. Lutsen, D. Vanderzande, P. Wagner, and T. J. Cleij, Sens. Actuators B **148**, 392–398 (2010).
[5] N. Bijnens, V. Vermeeren, M. Daenen, L. Grieten, K. Haenen, S. Wenmackers, O. A. Williams, M. Ameloot, M. vandeVen, L. Michiels, and P. Wagner, Phys. Status Solidi A **206**, 520–526 (2009).
[6] P. Cooreman, R. Thoelen, J. Manca, M. vandeVen, V. Vermeeren, L. Michiels, M. Ameloot, and P. Wagner, Biosens. Bioelectron. **20**, 2151–2156 (2006).
[7] F. Frederix, K. Bonroy, W. Laureyn, G. Reekmans, A. Campitelli, W. Dehaen, and G. Maes, Langmuir **19**, 4351–4357 (2003).
[8] A. Poghossian, D.-H. Mai, Yu. Mourzina, and M. J. Schöning, Sens. Actuators B **103**, 423–428 (2004).
[9] A. Poghossian, M. H. Abouzar, F. Amberger, D. Mayer, Y. Han, S. Ingebrandt, A. Offenhäuser, and M. J. Schöning, Biosens. Bioelectron. **22**, 2100–2107 (2006).
[10] M. Krämer, M. Pita, J. Zhou, M. Ornatska, A. Poghossian, M. J. Schöning, and E. Katz, J. Phys. Chem. C **113**, 2573–2579 (2009).
[11] Analog Devices, Datasheet AD 5933, http://www.analog.com/static/imported-files/data_sheets/AD5933.pdf.
[12] B. van Grinsven, T. Vandenryt, S. Duchateau, A. Gaulke, L. Grieten, R. Thoelen, S. Ingebrandt, W. De Ceuninck, and P. Wagner, Phys. Status Solidi A **297**, 919–923 (2010).
[13] Future Technologies Devices International, Datasheet FT232R, http://www.ftdichip.com/Support/Documents/DataSheets/ICs/DS_FT232R.pdf.
[14] C. H. Fry and R. I. Jabr, Surgery **28**, 49–54 (2010).
[15] J. Kafka, O. Pänke, B. Abendroth, and F. Lisdat, Electrochim. Acta **53**, 7467–7474 (2008).

 

[16] S. Zheng, M. S. Nandra, C.-Y. Shih, W. Li, and Y.-C. Tai, Sens. Actuators A **145/146**, 29–36 (2008).
[17] D. Berdat, A. Marin, F. Herrera, and M. A. M. Gijs, Sens. Actuators B **118**, 53–59 (2006).
[18] M. Thein, F. Asphahana, A. Cheng, R. Buckmaster, M. Zhang, and J. Xu, Biosens. Bioelectron. **25**, 1963–1969 (2010).
[19] Maxim Integrated Products, Datasheet DS 1077, http://datasheets.maxim-ic.com/en/ds/DS1077.pdf.
[20] C. A. Marquette, I. Lawrence, C. Polychronakos, and M. F. Lawrence, Talanta **56**, 763–768 (2002).
[21] K. Haupt and K. Mosbach, Chem. Rev. **100**, 2495–2504 (2000).
[22] R. Vansweevelt, A. Malesevic, M. Van Gompel, A. Vanhulsel, S. Wenmackers, J. D'Haen, V. Vermeeren, M. Ameloot, L. Michiels, C. Van Haesendonck, and P. Wagner, Chem. Phys. Lett. **485**, 196–201 (2010).
[23] O. A. Williams, M. Daenen, J. D'Haen, K. Haenen, J. Maes, V. V. Moshchalkov, M. Nesládek, and D. M. Gruen, Diamond Relat. Mater. **15**, 654–658 (2006).
[24] P. Christiaens, V. Vermeeren, S. Wenmackers, M. Daenen, K. Haenen, M. Nesládek, M. vandeVen, M. Ameloot, L. Michiels, and P. Wagner, Biosens. Bioelectron. **22**, 170–177 (2006).
[25] E. Gheeraert, S. Koizumi, T. Teraji, H. Kanda, and M. Nesládek, Diamond Relat. Mater. **9**, 948–951 (2000).
[26] J. Chhabra, Y.-Z. Li, H. Alkhouri, A. E. Blake, Q. Ge, C. L. Armour, and J. M. Hughes, Eur. Respir. J. **29**, 861–870 (2007).
[27] R. Y. Lin, L. B. Schwartz, A. Curry, G. R. Pesola, R. J. Knight, H. S. Lee, L. Bakalchuk, C. Tenenbaum, and R. E. Westfal, J. Allergy Clin. Immunol. **106**, 65–71 (2000).
[28] G. Barbara, V. Stanghellini, R. De Giorgio, C. Cremon, G. S. Cottrel, D. Santini, G. Pasquinelli, A. M. Morselli-Labate, E. F. Grady, N. W. Bunnett, S. M. Collins, and R. Corinalidesi, Gastroenterology **126**, 693–702 (2004).
[29] S. A. Piletsky, S. Alcock, and A. P. F. Tuner, Trends Biotechnol. **19**, 9–12 (2001).
[30] S. Arndt, J. Seebach, K. Psathaki, H.-J. Galla, and J. Wegener, Biosens. Bioelectron. **19**, 583–594 (2004).